Journal of The Electrochemical Society, **147** (7) 2805-2813 (2000)
S0013-4651(99)05-076-4 CCC: $7.00 © The Electrochemical Society, Inc.

Selective External Oxidation of the Intermetallic Compound, $BaAg_5$

Sitaraman Vilayannur, Kenneth H. Sandhage, and Suliman Dregia

Department of Materials Science and Engineering, The Ohio State University, Columbus, Ohio 43210, USA

The selective oxidation of $BaAg_5$ has been examined at 650-680°C in flowing 3%H_2/Ar ($p_{O_2} \leq 1.1 \times 10^{-19}$ atm). Under these conditions, a continuous external barium oxide scale formed. Depletion of Ba from the underlying $BaAg_5$ led to the formation of a continuous Ag layer between the oxide scale and the $BaAg_5$. Ba was only detected along grain boundaries in the continuous Ag layer, which was consistent with the negligible solubility reported for Ba in bulk Ag. The local thickness of the continuous Ag layer was inversely correlated to the local Ag grain size. Subsequent experiments with Ag-clad $BaAg_5$ revealed that surface oxide formation commenced at exposed Ag grain boundaries. $BaAg_5$ specimens clad with fine grained Ag foil exhibited more extensive oxide formation in a given time than specimens clad with coarse grained Ag foil. These observations confirmed that outward Ba migration through the continuous Ag layer occurred preferentially along Ag grain boundaries. This work demonstrates that an intermetallic compound may undergo external oxidation even when a continuous metallic (or intermetallic) layer, that possesses a low solubility for the oxidizable element, forms under the oxide scale.

Manuscript submitted May 18, 1999; revised manuscript received March 20, 2000.

Under conditions where the oxide of only one component of an intermetallic compound is thermodynamically stable, a continuous external oxide scale may form if the rate of outward migration of the oxidizable component to the intermetallic/oxide interface is sufficiently high.[1,2] During such external oxidation, the intermetallic compound will become selectively depleted of the oxidizable element. If the intermetallic compound possesses a very limited solid solution range, as is often the case, then such depletion can result in the formation of one or more metallic or intermetallic layers between the external oxide layer and the virgin intermetallic compound.[1] The oxidizable element must be able to migrate through such a continuous metallic or intermetallic layer at a sufficient rate in order to maintain the growth of the external oxide scale (*i.e.*, to avoid the formation of internal oxide particles).[1-3]

The selective oxidation of metallic solid solutions based on silver and other noble elements (Au, Pd, Pt) has received considerable attention.[3-31] Much less work, however, has been conducted on the selective oxidation behavior of noble-metal-bearing intermetallic compounds. The selective, external oxidation of high melting, Ir-based intermetallic compounds has been examined by a few authors.[32,33] Such Ir-based compounds have been evaluated for possible use as high temperature structural components for supersonic aircraft, rockets, missiles, and spacecraft.[34] Lee and Worrell examined the oxidation kinetics and microstructural evolution of Hf-Ir and Al-Ir intermetallic compounds (and two-phase mixtures of such intermetallic compounds) at 1550-1800°C at various oxygen partial pressures.[32] Continuous external HfO_2 and Al_2O_3 scales were observed to form on Ir-bearing compositions with >50 atom % Hf and >55 atom % Al, respectively. Chou examined the microstructural evolution of IrAl during oxidation at ≥1300°C in air.[33] After exposure for 8 h to air at 1300°C, an external Al_2O_3 layer was detected that was separated from the underlying IrAl alloy by an intermediate Ir-rich layer. After 100 h of oxidation at 1300°C, alternating Al_2O_3 and Ir-rich layers were observed. Such layer formation was attributed by Chou to the sluggish rate of outward Al diffusion relative to the rate of inward oxygen diffusion through the Ir-rich layer.[33]

In this paper, the selective external oxidation behavior of a noble-metal-rich intermetallic compound, $BaAg_5$, has been examined. The formation of an external barium oxide layer on $BaAg_5$ will cause this intermetallic compound to become depleted of Ba. Such Ba depletion is likely to result in the formation of a continuous Ag layer under the oxide, since (*i*) the $BaAg_5$-type compound possesses a limited solid solution range (see Fig. 1) and (*ii*) the $BaAg_5$-type compound is the most Ag-rich intermetallic compound in the Ag-Ba system.[35] The outward Ba permeability through such a Ag layer must remain relatively high, compared to the inward permeability of oxygen, in order to continue forming an external Ba oxide scale.[3] Because BaO is a relatively stable oxide, the oxidation of $BaAg_5$ can be conducted at very low oxygen partial pressures, where the inward permeability of oxygen through Ag can be greatly reduced.[36-38] However, since bulk Ag is reported to exhibit negligible solubility for Ba, it was not clear whether Ba transport through a continuous noble Ag layer could be sufficiently fast as to allow for sustained formation of a continuous external oxide scale.[35] This differs from the prior work on the external oxidation of IrAl, where a noble Ir layer with an appreciable solubility for Al forms under the Al_2O_3 scale at ≥1300°C.[32] The purpose of the present paper is to evaluate the selective external oxidation behavior of $BaAg_5$ at low oxygen partial pressures and to compare such behavior to prior work on Ir-bearing intermetallic compounds.

Experimental

Specimen preparation.—A dense ingot of $BaAg_5$ was produced by induction melting. A 60-70 g charge was prepared by blending Ba granules (99.7% purity, 2.5 cm average diam, Johnson Matthey, Inc.,

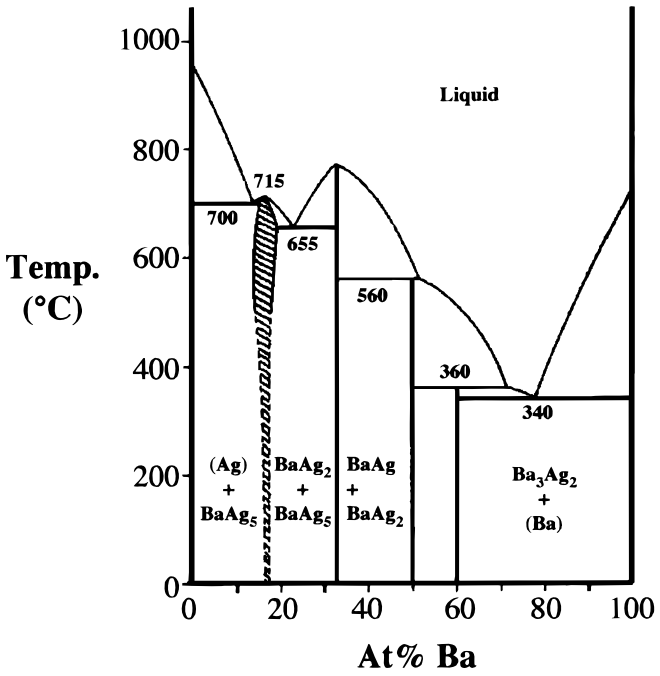

Figure 1. The Ag-Ba binary constitution phase diagram.[35]

S0013-4651(99)05-076-4 CCC: $7.00

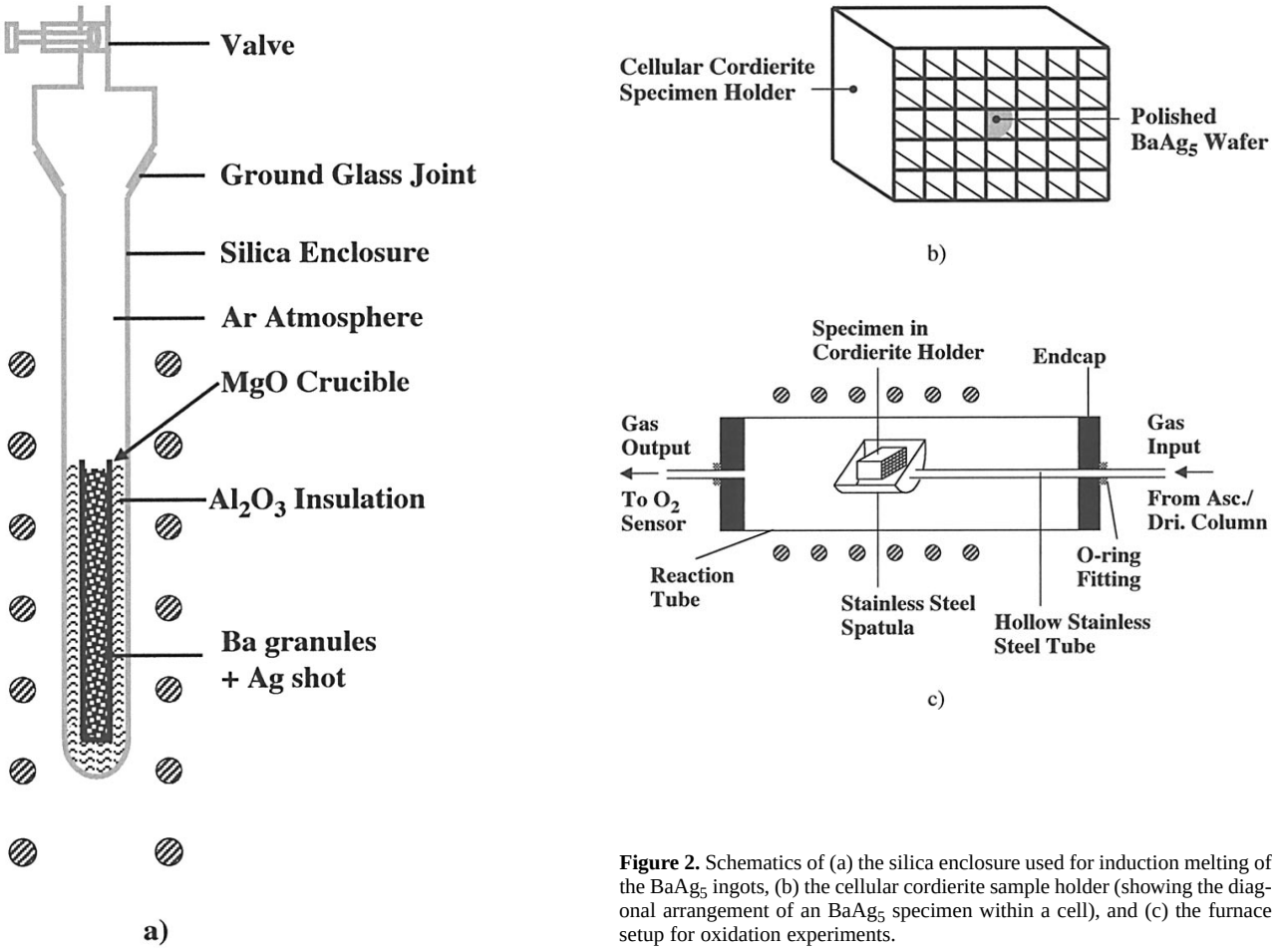

Figure 2. Schematics of (a) the silica enclosure used for induction melting of the $BaAg_5$ ingots, (b) the cellular cordierite sample holder (showing the diagonal arrangement of an $BaAg_5$ specimen within a cell), and (c) the furnace setup for oxidation experiments.

Ward Hill, MA) and Ag shot (99.9% purity, ≤3 mm diam, Johnson Matthey, Inc.) in the atomic ratio Ba:Ag = 1:4.7 (a slight excess of Ba was used to compensate for some Ba loss by evaporation during induction melting). The charge was placed within a cylindrical magnesia crucible (1.9 cm internal diam, 15.8 cm internal length, 94.8% relative density, 99.4% purity, Ozark Technical Ceramics, Webb City, MO) and sealed within a silica tube enclosure, as shown in Fig. 2a. In order to minimize tarnishing of the Ba prior to and during heatup, the blending and sealing were conducted within a glove box purged with Ar tapped from a liquid Ar tank. Prior to entry into the glove box, the Ar was passed through a packed column of Drierite (W. A. Hammon Drierite Co., Xenia, OH) and Ascarite II (Thomas Scientific, Swedesboro, NJ) and a model MO-5 Dri-Train gas purification system (Vacuum/Atmospheres Co., Hawthorne, CA) to remove residual water vapor, carbon dioxide, and oxygen, respectively. The oxygen content of the Ar-purged glove box was maintained at ≤0.1 ppm, as indicated by a stabilized zirconia oxygen sensor (model TM-1B, Ametek, Inc., Pittsburgh, PA). The sealed enclosure was placed inside a water-cooled copper coil (11.4 cm internal diam, 13.3 cm height, 7 turns) connected to an induction power supply (model VSG10, Balzers, Inc., Rochester, NY). The charge was melted and stirred with the power supply operating at 9600 Hz and 5 kV for 5 min followed by 10 kV for 10 min. The power supply was then turned off and the melt was allowed to cool to room temperature. Upon solidification, the ingot separated cleanly from the magnesia crucible. The ingot was sectioned into cylinders by electrical discharge machining under a bath of Rust-lick EDM-250 (ITW Fluid Products Group, Tustin, CA) and then cut into 1.5 mm thick × 5-8 mm diam wafers with a diamond saw. The large area surfaces of the wafers were polished with a series of diamond pastes in kerosene to a surface finish of 0.25 μm prior to oxidation.

Ag foil was bonded to some of the polished $BaAg_{5\pm x}$ wafers prior to oxidation. The as-received Ag foil (27.3±1.6 μm thickness, 99.9% purity, Johnson Matthey, Inc.) was first annealed at 400°C for 1 h to allow for recrystallization to a fine grain size. Some of the Ag foil was further annealed for 24 h at 840°C to allow for extensive grain growth. Ag foils of each type were then bonded to $BaAg_{5\pm x}$ wafers under a modest uniaxial stress of 0.1 MPa during heating to 500°C in an Ar atmosphere.

Oxidation processing.—Selective oxidation of the $BaAg_5$ and Ag-clad $BaAg_5$ specimens was conducted at 650-680°C in a flowing 3%H_2/Ar gas mixture within a controlled atmosphere horizontal tube furnace. The specimens were placed diagonally within the channels of a cellular cordierite honeycomb substrate (Corning, Inc., Corning, NY) so as to expose both large area surfaces to the reaction gas (see Fig. 2b). Pt mesh was wrapped around both open ends of the cordierite honeycomb to act as a catalyst for the reaction of hydrogen with residual oxygen in the furnace. The honeycomb substrate was placed on a stainless steel scoop that was welded onto a hollow stainless steel tube (see Fig. 2c). The tube was sealed by an O-ring fitting to a port in the endcap at the end of the reaction tube. Prior to the start of an oxidation experiment, the specimen was positioned near the endcap within the reaction tube (*i.e.*, well outside of the heated zone of the furnace). The furnace was then heated and the reaction tube was purged with the 3%H_2/Ar gas mixture. Measurements with a zirconia oxygen sensor revealed that the oxygen partial pressures within the tube furnace during steady-state flow of the 3%H_2/Ar gas mixture at 650 and 680°C were $1.5 \pm 0.7 \times 10^{-20}$ atm and $1.1 \pm 0.6 \times 10^{-19}$ atm, respectively. After the furnace achieved the targeted temperature and oxygen partial pressure, the specimen-bearing cordierite substrate was thrust into the hot zone of the fur-

S0013-4651(99)05-076-4 CCC: $7.00

nace. By using the O-ring sealed stainless steel scoop, the specimens could be inserted in and out of the hot zone while under a controlled atmosphere. At the end of the oxidation treatment, the specimen was quickly retracted back to the initial, cool position near the endcap. No evidence of a reaction between the specimen and the cordierite substrate was detected (*i.e.*, the specimen did not adhere to the cordierite, and the cordierite was not stained by the specimen).

Chemical and microstructural characterization.—The density of the as-cast Ba-Ag ingot was measured by Archimede's method with hexane as the buoyant fluid. The bulk composition of the Ba-Ag ingot was evaluated with inductively coupled plasma optical emission spectroscopy (ICP-OES, Optima 3000, The Perkin-Elmer Corp., Norwalk, CT). Specimens for ICP-OES analyses were prepared by dissolution into an aqueous solution containing 5 vol % nitric acid and 5 vol % hydrofluoric acid. The nominal Ag and Ba concentrations of such solutions were 18.9 and 4.8 ppm (by weight), respectively. ICP-OES analyses were conducted using the 243.779, 328.068, and 338.289 nm lines for Ag and the 230.424, 233.537, and 455.403 nm lines for Ba. The intensities of these lines were correlated to solution concentrations with the use of Ag and Ba solution standards of similar concentration as the specimen solutions. Chemical analyses were also conducted by wavelength dispersive spectroscopy (WDS) using an electron microprobe (model SX 50 EPMA, Cameca Instruments, Inc., Trumbull, CT). WDS analyses were used to evaluate local variations in the compositions of the Ba-Ag ingot and the oxidized specimens. WDS analyses were conducted with an electron beam operating at a voltage of 15 kV, a current of 20 nA, and a focused spot size of a few micrometers. Specimens for WDS analyses were prepared by mounting in epoxy, cross sectioning with a diamond wafering blade, and then polishing with a series of diamond pastes to a surface finish of 0.25 μm. WDS analyses were calibrated with the use of Ag and $BaSO_4$ standards. The external surfaces and polished cross sections of oxidized specimens were also examined with a scanning electron microscope (SEM, XL-30 FEG, Philips Electron Optics NV, Eindhoven, The Netherlands) equipped with an energy-dispersive X-ray detector (Si/Li detector, Edax International, Mahwah, NJ). Some of the polished cross sections of oxidized specimens were etched for 2 min using a 60 vol % HCl/40 vol % HNO_3 solution. Grain size analyses were then conducted on such etched specimens by the linear intercept method. Over 500 grains were examined by secondary electron imaging to obtain a reliable average.[39] Select oxidized samples were also characterized by transmission electron microscopy (TEM, model EM400T, Philips Electron Optics NV). TEM specimens were prepared by cutting thin foils from oxidized wafers, gluing the foils inside a 3 mm diam stainless steel tube, and then thinning the foils to electron transparency using standard grinding and ion milling procedures. The phase contents of the ingot and of the oxidized specimens were also evaluated with X-ray diffraction (XRD) analyses (Bragg-Brentano geometry). Powder diffraction specimens were prepared by grinding with an agate mortar and pestle within the Ar atmosphere glove box. Si powder was blended with specimen powders to act as an internal XRD standard. The powder mixture was mixed with X-ray transparent grease (high vacuum Si grease, Dow Corning, Inc., Midland, MI) within the glove box and spread onto a single crystal Si substrate. XRD patterns were also obtained from the external surfaces of oxidized specimens using Cu powder as an internal standard. XRD analyses (PAD-V system, Scintag, Inc., Cupertino, CA) were conducted with Cu Kα radiation using a beam voltage of 45 kV, a beam current of 20 mA, a 6° takeoff angle, and a scan rate of 0.5°/min.

Results

Characterization of the Ba-Ag ingot.—XRD analysis of powder obtained from the cast Ba-Ag ingot revealed all of the major diffraction peaks for hexagonal $BaAg_{5\pm x}$ (*i.e.*, with relative intensities in excess of a few percent).[40] Least squares fitting of the diffraction data yielded *a* and *c* lattice parameters of 5.776 and 4.608 Å, respectively, for hexagonal $BaAg_{5\pm x}$, which is consistent with the data of Bruzzone *et al*. for the composition $BaAg_{5.1\pm0.2}$.[35] Diffraction peaks for other Ba-Ag compounds (*e.g.*, $BaAg_2$, BaAg, Ba_3Ag_2), for metallic Ba, or for Ba-bearing oxides (*e.g.*, BaO, BaO_2, $BaCO_3$, $Ba(OH)_2$) were not detected.[35,40] Secondary electron images of polished ingot cross sections revealed a small number of isolated pores that were submicrometer in size. Backscattered electron images and X-ray maps revealed that the ingot was chemically homogeneous on the scale of a few micrometers. WDS analyses of the polished cross section yielded an average (10 randomly positioned analyses) composition of 16.0 ± 0.7 atom % Ba and 84.0 ± 0.7 atom % Ag. ICP-OES analysis yielded a similar overall composition of 15.9 atom % Ba and 84.1 atom % Ag for the bulk Ba-Ag ingot. The latter analyses corresponded to a mixture of 97.8 ± 0.2 vol % $BaAg_{5.1}$ and 2.2 ± 0.2 vol % Ag (or 85.3 ± 1.2 mol % $BaAg_{5.1}$ and 14.7 ± 1.2 mol % Ag).[a] Archimedes measurements yielded an average ingot density of 8.30 g/cm^3, which corresponded to 96.3% of the theoretical density (8.62 g/cm^3) of such a mixture.[35,40]

External oxidation of $BaAg_5$ specimens.—A dramatic change in the microstructure of the $BaAg_5$ specimens was observed after exposure to the 3%H_2/Ar gas mixture at 650-680°C. Secondary electron (SE) and backscattered electron (BSE) images, and associated X-ray maps for Ba and Ag, of a polished cross section of a specimen exposed for 24 h to the flowing 3%H_2/Ar gas mixture at 650°C are shown in Fig. 3. A continuous Ba oxide scale, containing discontinuous Ag particles, was detected on the surface of this specimen. This external scale was separated from the unoxidized $BaAg_5$ core by a continuous Ag-rich layer. Some isolated pores were also detected within this Ag-rich layer. A composition profile obtained by conducting a series of WDS point analyses across the oxide and Ag-rich layers is shown in Fig. 4. The external oxide and intermediate Ag-rich layer were comprised of essentially pure barium oxide and pure Ag, respectively.[b] Similar microstructural features were observed in specimens annealed in the 3%H_2/Ar gas mixture at 680°C.

Although the thicknesses of the external oxide and underlying Ag layers tended to increase with oxidation time, considerable variations in thickness were observed within a given oxidized sample. Indeed, such thickness variations made it impossible to fit, with any real confidence, simple kinetic laws to the thickening rate data for the oxide and Ag layers. SE images of relatively thick and thin regions of the continuous Ag layer formed on a $BaAg_5$ specimen during oxidation in 3%H_2/Ar for 24 h at 650°C are shown in Fig. 5a and b, respectively. These images were obtained after etching the polished cross section in a 60 vol % HCl/40 vol % HNO_3 solution to reveal the Ag grains within the continuous Ag layer. Higher magnification SE images of the grains within the relatively thick and thin Ag layers of Fig. 5a and b are shown in Fig. 5c and d, respectively. Although the grains in the continuous Ag layer were submicrometer in size, a larger fraction of relatively coarse grains were detected at locations where the Ag layer was relatively thin (Fig. 5d). The average size of the grains in the continuous silver layer at the location shown in Fig. 5a and c was 0.27 μm, whereas the average grain size at the location shown in Fig. 5b and d was 0.45 μm.

TEM analyses were used to examine the grain boundaries within the continuous Ag layer. After oxidation for 72 h at 680°C in a 3%H_2/Ar atmosphere, the external oxide scale formed on one side of the $BaAg_5$ wafer was removed by polishing with 1200 grit SiC paper. Further polishing and ion beam thinning was conducted from the other side of the specimen, so that electron transparent regions were produced within the continuous Ag layer. A bright field TEM

[a] For brevity, these $BaAg_{5.1}$-bearing specimens herein are simply referred to as $BaAg_5$ specimens.

[b] The measured gradients in concentration near the oxide/Ag and Ag/$BaAg_5$ interfaces are likely to be less steep than the actual gradients, owing to (*i*) overlap of the beam interaction volume with both oxide and Ag or Ag and $BaAg_5$ phases when the beam was located very close to the oxide/Ag or Ag/$BaAg_5$ interfaces, respectively, (*ii*) the discrete step distances between spot analyses (5 μm), and (*iii*) the roughnesses of the oxide/Ag and Ag/$BaAg_5$ interfaces (*i.e.*, the interface position below the polished surface may not have been the same as observed on the specimen surface).

S0013-4651(99)05-076-4 CCC: $7.00

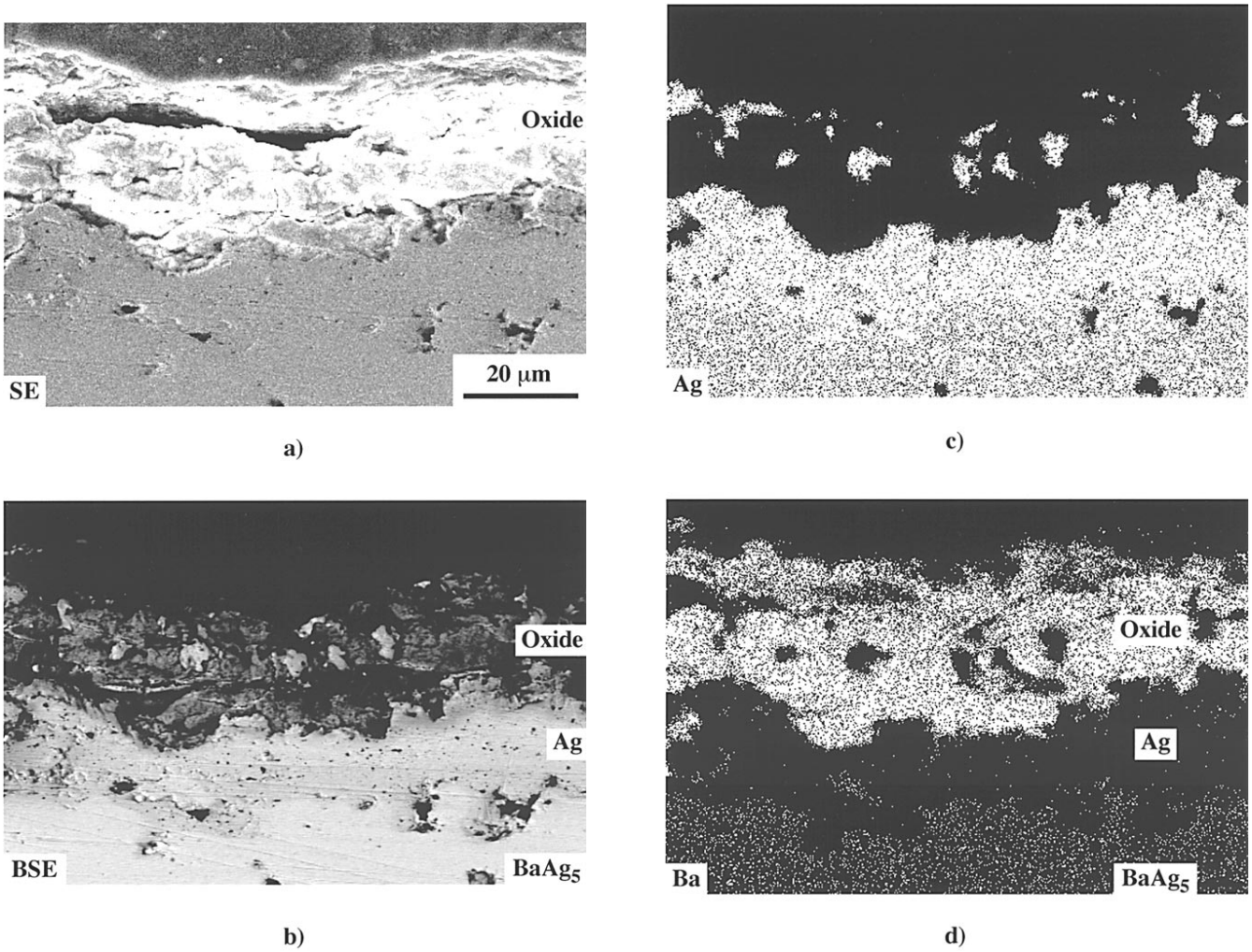

Figure 3. (a) Secondary and (b) backscattered electron images of a polished cross section of a $BaAg_5$ specimen that had been exposed for 24 h to the flowing $3\%H_2$/Ar mixture at 650°C. X-ray maps for Ag and Ba, associated with the images in a and b, are shown in (c) and (d), respectively.

image of a grain boundary within the silver layer is shown in Fig. 6a. A Ba-rich phase was detected in the grain boundary regions between Ag grains, as indicated by the energy-dispersive spectrometry (EDS) pattern in Fig. 6b.[c]

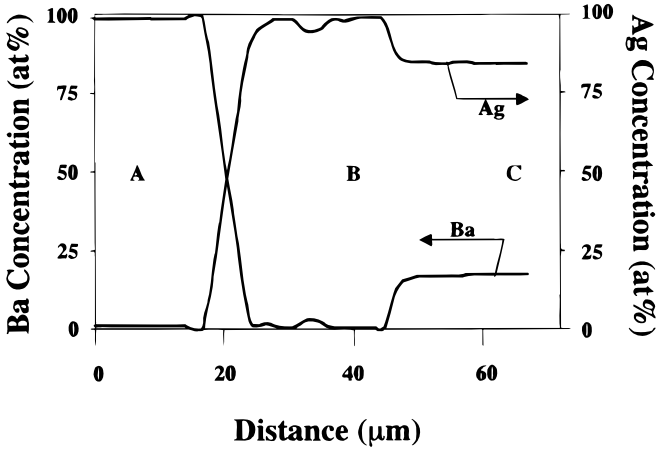

Figure 4. A composition profile generated from a linear series of WDS (EPMA) point analyses (with 5 μm steps between analyses) conducted on a polished cross section of a $BaAg_5$ specimen that had been exposed for 24 h to the flowing $3\%H_2$/Ar mixture at 650°C. The regions A, B, and C refer to the locations of the external oxide scale, the continuous Ag layer, and the underlying $BaAg_5$, respectively.

External oxidation of Ag-clad, $BaAg_5$ specimens.—SE images of external surfaces of Ag-clad, $BaAg_5$ specimens are shown in Fig. 7a and b. Linear intercept analyses indicated that the average grain sizes of the silver foils bonded to the specimens of Fig. 7a and b were 82.5 and 5.5 μm, respectively. SE and BSE images of the external surfaces of Ag-clad, $BaAg_5$ specimens after exposure to the $3\%H_2$/Ar gas mixture at 680°C for 1 h are shown in Fig. 8a-d. The specimens in Fig. 8a and b were clad with the relatively fine grained silver foil (of the type shown in Fig. 7b), whereas the specimens in Fig. 8c and d were clad with the relatively coarse grained Ag foil (of the type shown in Fig. 7a). After the 1 h oxidation treatment, the grain boundaries of the Ag foil were decorated with oxide particles. The coverage of the surface with oxide was more extensive for the specimens clad with fine grained Ag than for specimens clad with relatively coarse-grained Ag. A representative EDS analyses obtained from one of the oxide particles at an Ag grain boundary is shown in Fig. 8e. The particle was enriched in Ba and oxygen. SE and BSE images of the external surfaces of Ag-clad $BaAg_5$ specimens after exposure for 18 h to the $3\%H_2$/Ar gas mixture at 680°C are shown in Fig. 9a-d. The external surface of the fine-grained, Ag-bonded specimen was nearly completely covered with oxide, whereas much

[c] The modest C and oxygen peaks detected in Fig. 6b were attributed to the formation of some $BaCO_3$ upon exposure of the specimen to ambient air during transfer from the Ar ion mill to the TEM.

S0013-4651(99)05-076-4 CCC: $7.00 © The Electrochemical Society, Inc.

less oxide was observed on the surface of the coarse grained, Ag-bonded specimen. In the latter specimen, the oxide was largely confined to Ag grain boundaries.

Discussion

In order to reduce the inward oxygen permeability and enhance the likelihood for external oxidation, $BaAg_5$ specimens were exposed to flowing H_2/Ar gas mixtures at 650-680°C ($p_{O_2} = 1.5 \pm 0.7 \times 10^{-20}$ to $1.1 \pm 0.6 \times 10^{-19}$ atm). Oxidation at such low oxygen partial pressures did indeed result in the formation of an external Ba oxide scale (Fig. 3). Owing to the limited solid solution range of bulk $BaAg_{5\pm x}$ (see Fig. 1), the depletion of Ba from the underlying $BaAg_5$-type phase resulted in the formation of a continuous Ag layer immediately below the external oxide.[35] The morphology shown in Fig. 3 was similar to that reported by Chou for the oxidation of IrAl (the most Ir-rich intermetallic compound) for 8 h at 1300°C in air.[33] In the latter case, an Ir-rich layer had formed between an external Al_2O_3 scale and the underlying IrAl alloy. However, while iridium possesses appreciable bulk solubility for aluminum at 1300°C (on the order of 10 atom %), the solubility of barium in a bulk silver lattice is reported to be negligible.[32,35] Hence, while aluminum could dissolve into and migrate through the grains in the continuous Ir layer formed during the oxidation of IrAl at 1300°C, a similar lattice transport mechanism was unlikely to have been operative in the present work due the lack of appreciable Ba solubility in bulk Ag at 650-680°C.

In order to allow for continued growth of the external barium oxide scale, Ba transport through the continuous Ag layer is likely to have occurred by an alternate (nonlattice) path. The formation of a relatively thick Ag layer at locations where the Ag grains were relatively fine (Fig. 5a-d) suggested that Ba migration through the Ag was occurring preferentially along Ag grain boundaries. Additional evidence for this transport mechanism was provided by TEM analyses (Fig. 6) which revealed the presence of Ba along grain boundaries in the continuous Ag layer. In order to confirm such a transport mechanism, experiments were conducted with $BaAg_5$ specimens clad with Ag layers possessing significantly different grain sizes (5.5 ± 1.5 μm or 82.5 ± 11.7 μm). After oxidation for 1 h at 680°C in the H_2/Ar gas mixture, barium oxide particles were observed to have formed preferentially on the exposed Ag grain boundaries of the clad $BaAg_5$ specimens (Fig. 8a-d). The extent of surface coverage by barium oxide was greater for the specimen clad with fine Ag than for the coarse Ag-clad specimen. This difference in surface coverage became even more obvious after oxidation under similar conditions for 18 h (Fig. 9a-d). The increase in the extent of barium oxide formation at the external Ag surface with decreasing Ag grain

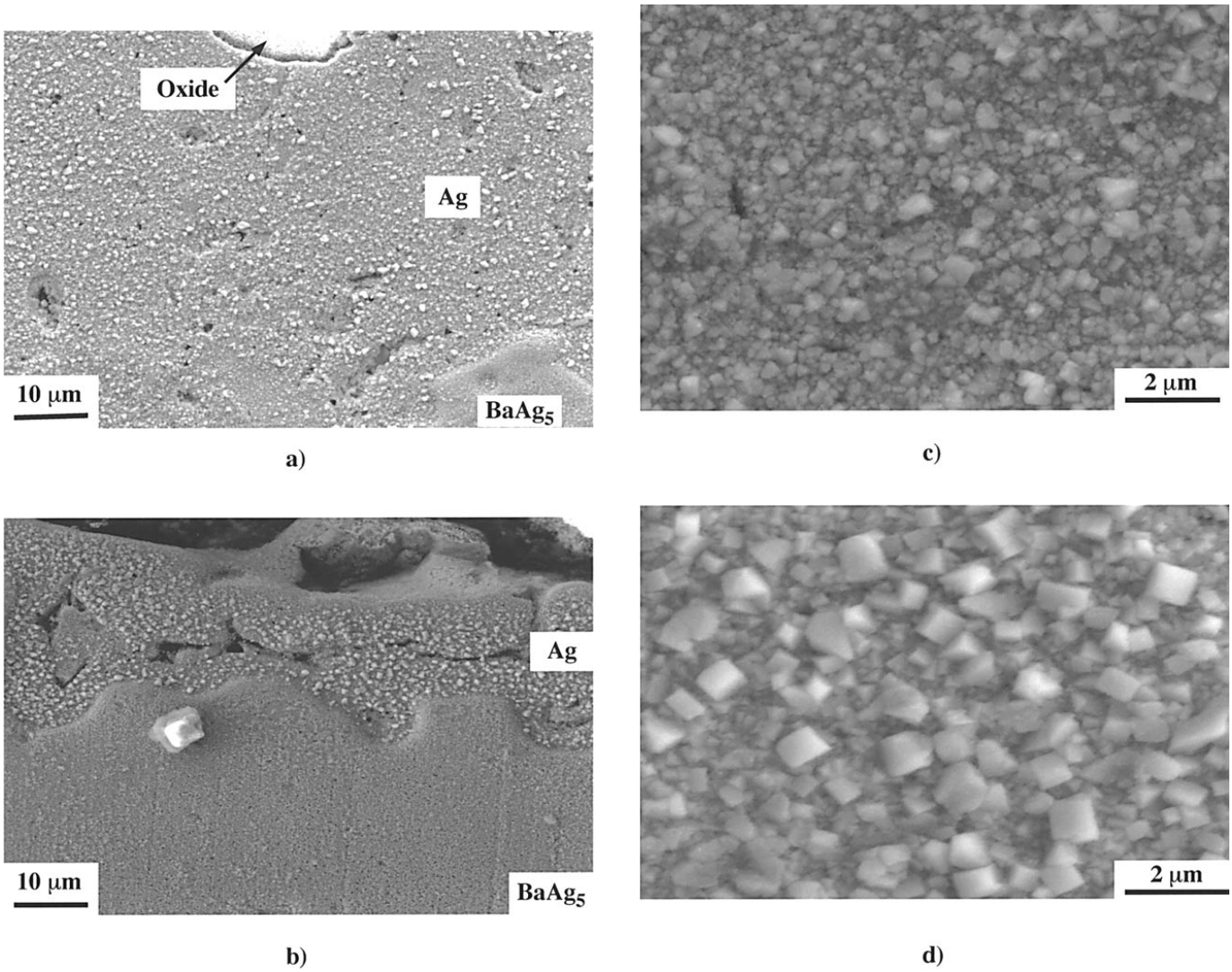

Figure 5. Secondary electron images of polished and etched cross sections revealing: (a) relatively thick and (b) relatively thin sections of the continuous Ag layer formed on the same $BaAg_5$ specimen during exposure for 24 h to the flowing 3%H_2/Ar mixture at 650°C (note: the oxide scale had spalled away from the Ag layer in b). Higher magnification secondary electron images obtained from the regions shown in a and b are shown in (c) and (d), respectively.

S0013-4651(99)05-076-4 CCC: $7.00

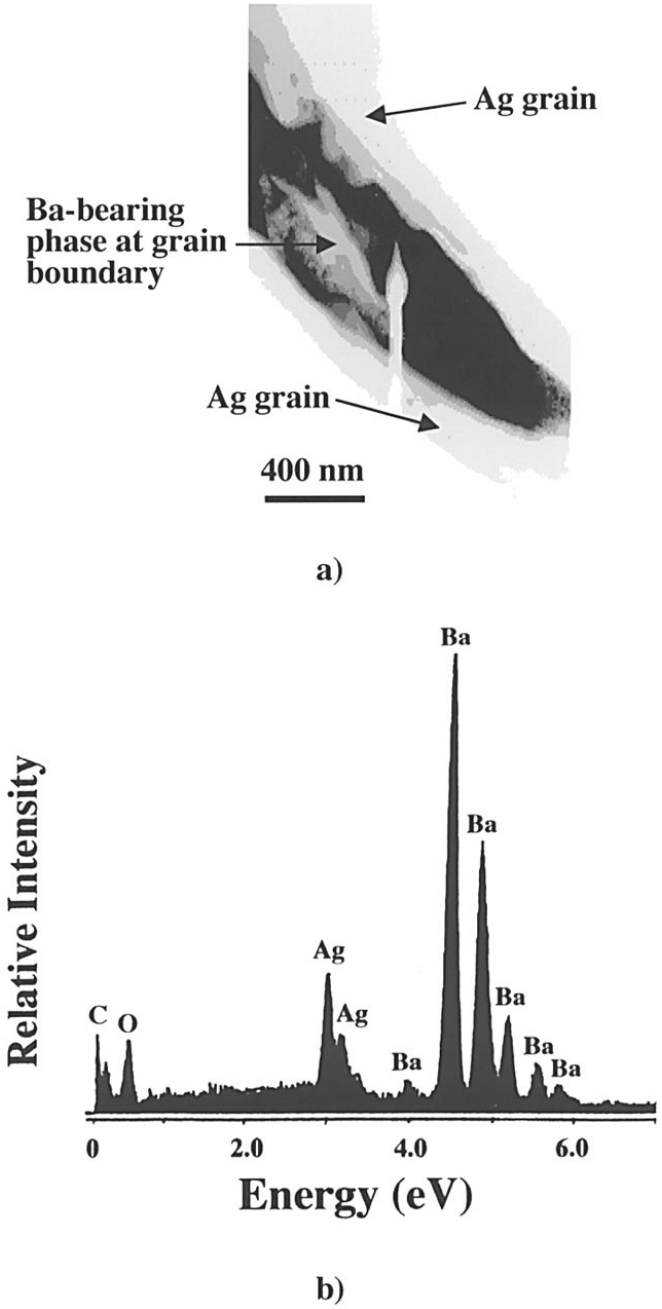

Figure 6. (a) Bright field TEM image of a Ba-rich phase located at a grain boundary in the continuous silver layer generated upon exposure of a $BaAg_5$ specimen to the flowing 3%H_2/Ar mixture for 72 h at 650°C. (b) An EDS pattern obtained from the Ba-rich phase shown in a.

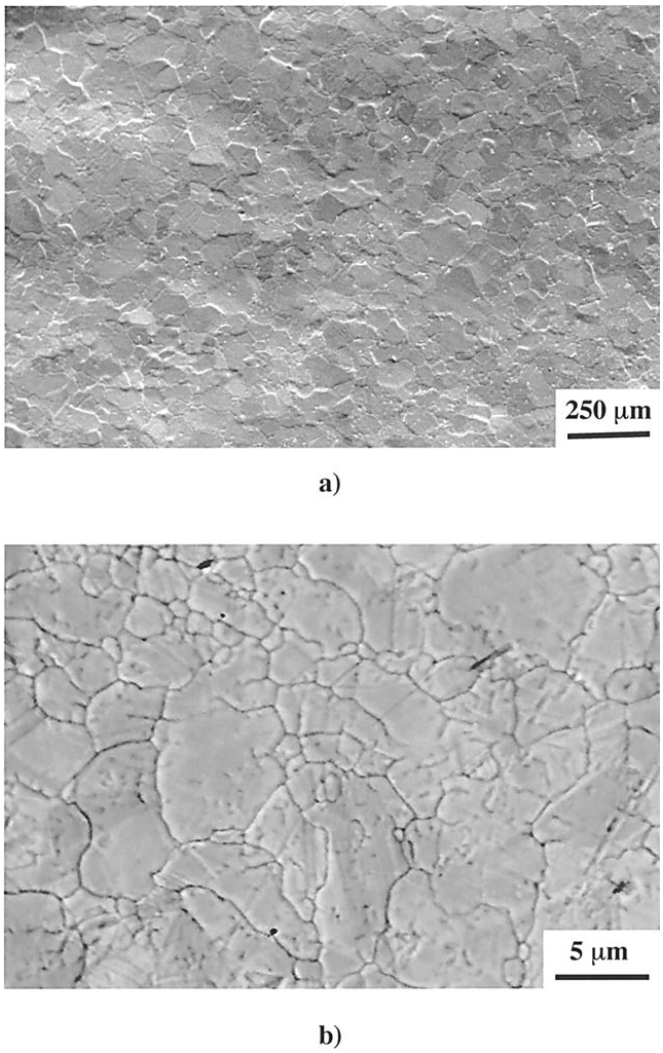

Figure 7. Secondary electron images of the external surfaces of Ag-clad $BaAg_5$ specimens. The average sizes of the Ag grains in (a) and (b) were 82.5 and 5.5 μm, respectively.

size, coupled with the preferred formation of oxide particles on exposed Ag grain boundaries during short-term oxidation, provided unambiguous proof that Ag grain boundaries were acting as preferred transport paths for Ba during the external oxidation of $BaAg_5$ specimens at 650-680°C in the H_2/Ar gas mixtures.

Although such a transport mechanism (metal migration along grain boundaries in a subsurface metallic layer) has not been previously reported for the external oxidation of intermetallic compounds, an analogous mechanism was reported by White and Liu for the selective external oxidation of Th-doped, Ir-0.3% W alloys at 1330°C in low pressure (1.3×10^{-3} Pa) oxygen.[41] The Th was present in such alloys as isolated $ThIr_5$ particles in an Ir-rich matrix. White and Liu found that Th (generated by the dissociation of $ThIr_5$ particles) migrated outward along Ir alloy grain boundaries to the external surface and was oxidized to form discrete ThO_2 particles.[41] Given the observations of these authors and the negligible solubility reported for Th in Ir, [42] it seems likely that the oxidation of phase-pure $ThIr_5$ at 1330°C in low pressure oxygen (*i.e.*, so as to yield an external scale of the very high melting oxide, ThO_2) would proceed by a mechanism similar to that observed in the present work for $BaAg_5$.

As far as the present authors are aware, this paper is the first report of the selective external oxidation of an intermetallic compound involving rapid transport of the oxidizable solute element along the grain boundaries of a continuous, subsurface metallic layer. This observation is significant in that it demonstrates that an intermetallic compound may undergo external oxidation even when an underlying, solute-depleted metallic (or intermetallic) zone possesses negligible bulk solubility for the oxidizable solute element.

Conclusions

The selective oxidation of dense, polished wafers of the noble-metal-rich intermetallic compound, $BaAg_5$, has been examined at 650-680°C in 3%H_2/Ar gas mixtures ($p_{O_2} = 1.5 \pm 0.7 \times 10^{-20}$ to $1.1 \pm 0.6 \times 10^{-19}$ atm). Under these conditions, a continuous barium oxide scale formed on the external surface of the $BaAg_5$ specimens. The depletion of Ba underneath the external oxide scale, coupled with the limited solid solubility of Ag in $BaAg_{5\pm x}$, led to the formation of an underlying, continuous Ag layer. Considerable variation was detected in the thickness of the Ag layer within a given

S0013-4651(99)05-076-4 CCC: $7.00

sample, with relatively thick layers located at positions where the average Ag grain size was relatively fine. TEM analyses also revealed the presence of Ba along grain boundaries in the continuous Ag layer. These observations were consistent with the outward migration of Ba through the Ag layer along grain boundaries. Experiments conducted with $BaAg_5$ specimens clad with Ag layers of sig-

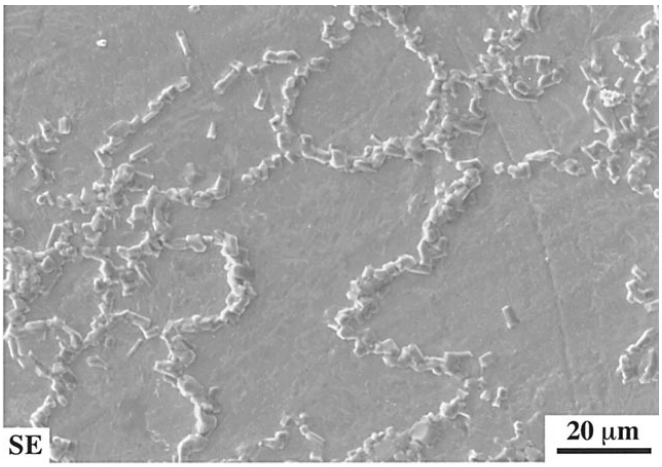

a)

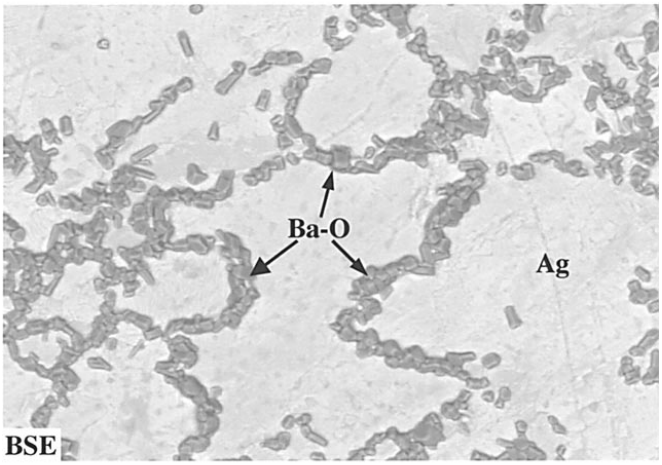

b)

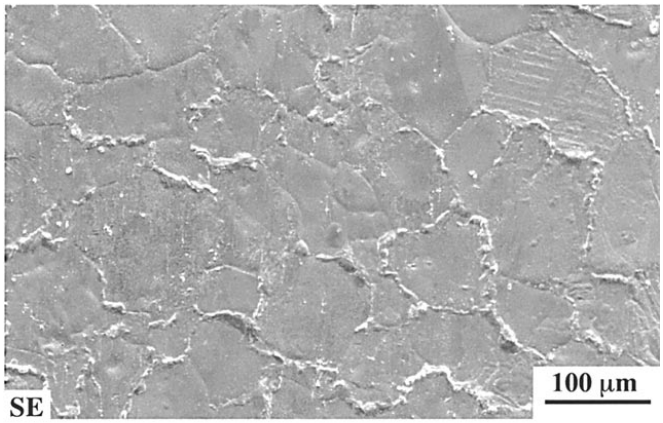

c)

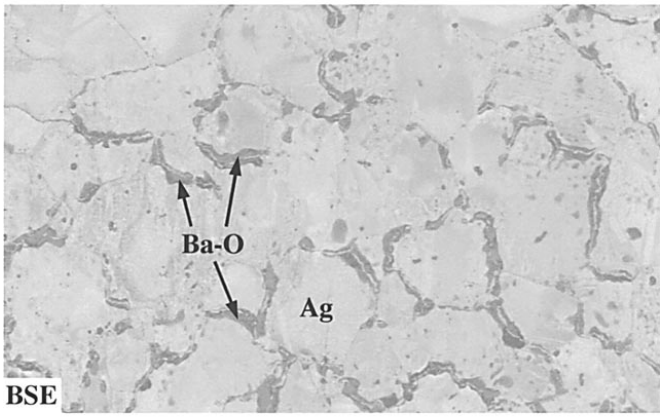

d)

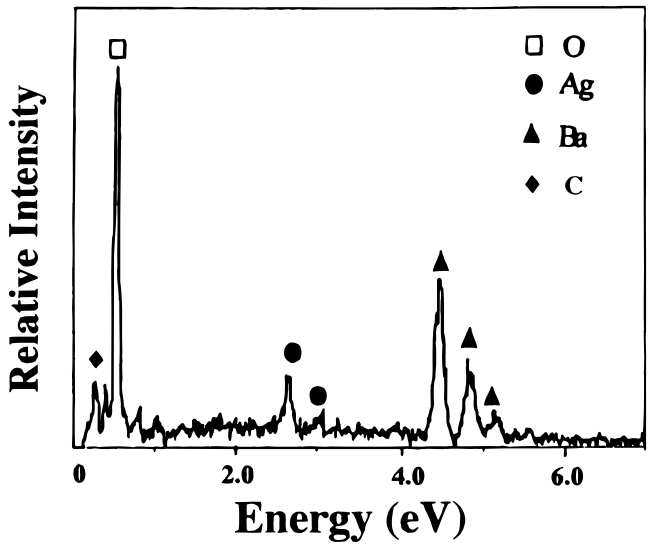

e)

Figure 8. (a) Secondary and (b) backscattered electron images of the external surface of a $BaAg_5$ specimen clad with fine grained (5.5 μm) Ag foil after exposure to the flowing 3%H_2/Ar mixture for 1 h at 680°C. (c) Secondary and (d) backscattered electron images of the external surface of a $BaAg_5$ specimen clad with coarse-grained (82.5 μm) Ag foil after exposure to the flowing 3%H_2/Ar mixture for 1 h at 680°C. (e) An EDS pattern obtained from an oxide particle located at a silver grain boundary of the specimen shown in a.

S0013-4651(99)05-076-4 CCC: $7.00

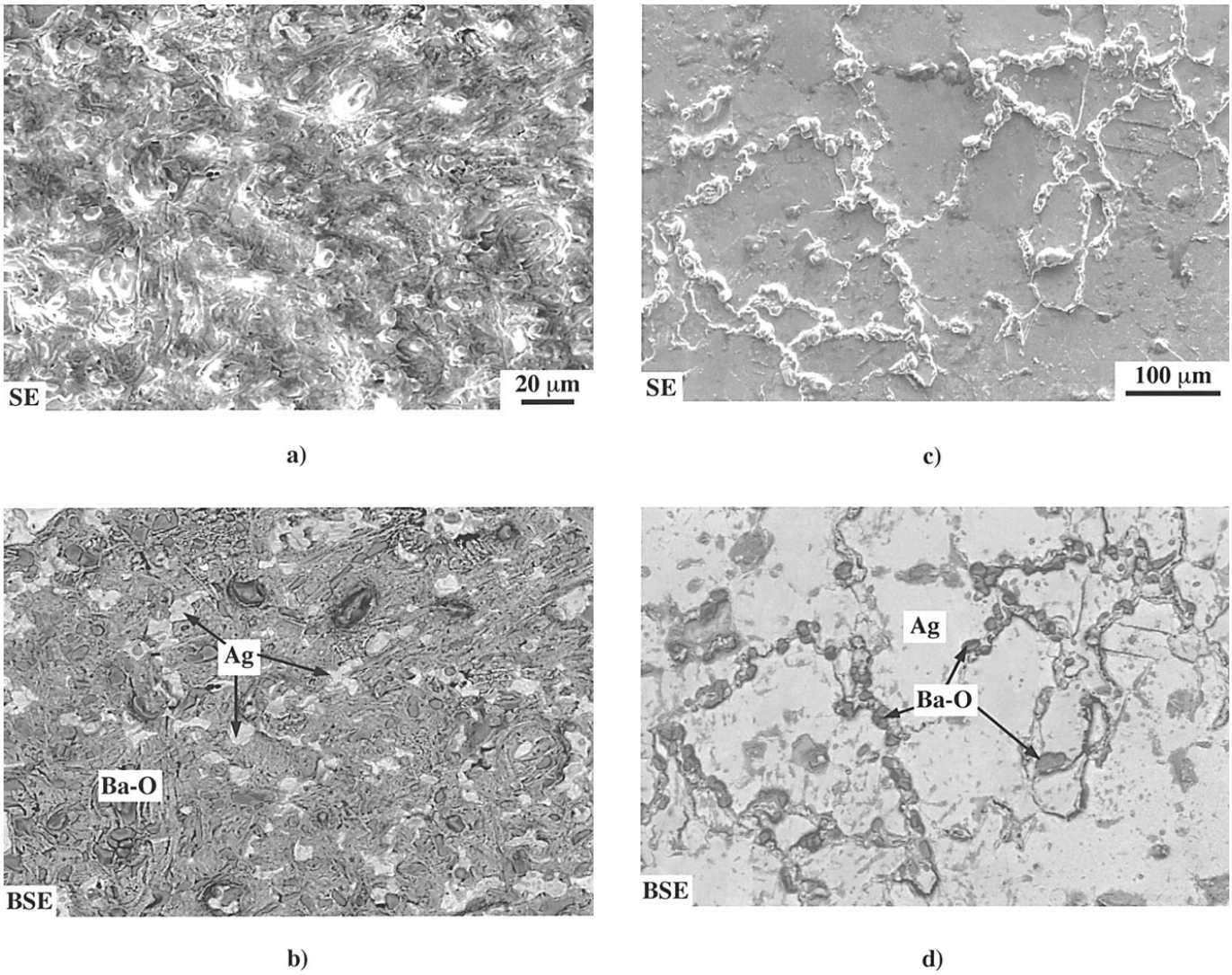

Figure 9. (a) Secondary and (b) backscattered electron images of the external surface of a $BaAg_5$ specimen clad with fine grained (5.5 μm) Ag foil after exposure to the flowing 3%H_2/Ar mixture for 18 h at 680°C. (c) Secondary and (d) backscattered electron images of the external surface of a $BaAg_5$ specimen clad with coarse grained (82.5 μm) Ag foil after exposure to the flowing 3%H_2/Ar mixture for 18 h at 680°C.

nificantly different grain size (5.5 *vs*. 82.5 μm) revealed that (*i*) after oxidation at 650°C for 1 h, barium oxide particles had formed preferentially at exposed Ag grain boundaries, and (*ii*) the surface coverage of barium oxide particles was much more extensive for the specimens clad with the Ag foil of finer grain size. These observations provided unambiguous proof that outward Ba migration through the continuous Ag layer occurred via a grain boundary transport mechanism. This work demonstrates that external oxidation of an intermetallic compound is possible even when a continuous metallic layer, with a low bulk solubility for the oxidizable element, forms between the oxide and the intermetallic compound.

Acknowledgments

The financial support provided by Midwest Superconductivity Consortium under grant no. DOE FG02-90ER45427 is gratefully acknowledged. Michael Comerford of Ohio State University is also thanked for technical help with EPMA.

The Ohio State University assisted in meeting the publication costs of this article.

References

1. G. H. Meier and F. S. Pettit, *Mater. Sci. Eng. A*, **153**, 548 (1992).
2. C. Wagner, *J. Electrochem. Soc.*, **99**, 369 (1952).
3. C. Wagner, *Z. Elektrochem.*, **63**, 772 (1959).
4. R. A. Rapp, *Corrosion*, **21**, 382 (1965).
5. J. L. Meijering, *Advances in Materials Research*, Vol. 5, H. Herman, Editor, p. 1, John Wiley & Sons, New York (1971).
6. D. L. Douglass, *J. Met.*, **43**, 74 (1991).
7. D. L. Douglass, *Oxid. Met.*, **44**, 81 (1995).
8. J. L. Meijering and M. J. Druyvesteyn, *Philips Res. Rep*., **2**, 81, 260 (1947).
9. J. E. Verfurth and R. A. Rapp, *Trans. Am. Inst. Min. Metall. Pet. Engs*., **230**, 1310 (1964).
10. L. Charrin, A. Combe, and J. Cabane, *Oxid. Met*., **37**, 65 (1992).
11. B. M. Semega, L. Charrin, A. Combe, and J. Aride, *Philos. Mag. A*, **66**, 1139 (1992).
12. A. Combe and J. Cabane, *Oxid. Met.*, **21**, 21 (1984).
13. G. Bohm and M. Kahlweit, *Acta Met.*, **12**, 641 (1964).
14. H. Spengler, *Metall.*, **17**, 710 (1963).
15. H. Spengler, *Metall.*, **20**, 721 (1966).
16. Y. S. Shen and R. H. Krock, *Matell. Trans.*, **5**, 312 (1974).
17. T. Igarashi, Y. Amano, and Y. Kodama, *Nippon Kinzoku Gakkaishi*, **44**, 501 (1980).
18. W. Segeth, D. O. Boerma, L. Niesen, J. R. Heringa, and A. Van Veen, *Z. Phys. B: Condens. Matter*, **73**, 43 (1988).
19. G. Elssner and E. Gebhardt, *Z. Metallkd.*, **60**, 922 (1969).
20. A. Verma and T. R. Anantharaman, *Bull. Mater. Sci.*, **14**, 1 (1991).
21. J. Takada, Y. Tomii, N. Yoshida, M. Sasaki, and M. Koiwa, *Oxid. Met.*, **37**, 13 (1992).
22. H. W. Pickering, *J. Electrochem. Soc.*, **119**, 641 (1972).
23. J. L. Meijering, *Z. Elektrochem.*, **63**, 824 (1959).
24. R. A. Rapp, D. F. Frank, and J. V. Armitage, *Acta Metall.*, **12**, 505 (1964).
25. R. A. Rapp, *Acta Metall*., **9**, 730 (1961).
26. H. Ohno, O. Miyakawa, K. Watanabe, and N. Shiokawa, *J. Dent. Res*., **61**, 1255

S0013-4651(99)05-076-4 CCC: $7.00

(1982).
27. H. Ohno, Y. Kanzawa, and I. Kawashima, *Dent. Mater. J.*, **3**, 36 (1984).
28. J. A. Eastman and M. Ruehle, *Ceram. Eng. Sci. Proc.*, **10**, 1515 (1989).
29. Y. Ning, Y. Li, and H. Dai, *Rare Met. (Beijing)*, **9**, 30 (1990).
30. E. I. Rytvin, V. A. Yastrebov, and L. E. Morozova, *Izv. Akad. Nauk. SSSR, Met.*, (4), 184 (1989).
31. E. I. Daneliya, M. I. Doperchuk, and G. I, Kandyba, *Izv. Akad. Nauk. SSSR, Met.*, (4), 181 (1989).
32. K. N. Lee and W. L. Worrell, *Oxid. Met.*, **32**, 357 (1989).
33. T. C. Chou, *J. Mater. Res.*, **5**, 378 (1990).
34. D. W. McKee and R. L. Fleischer, *Mater. Res. Soc. Symp. Proc.*, **213**, 969 (1991).
35. G. Bruzzone, M. Ferretti, and F. Merlo, *J. Less-Common Met.*, **128**, 259 (1987).
36. I. Barin, *Thermochemical Data of Pure Substances*, p. 12, 148, 149, VCH Verlagsgesellschaft, Weinheim, Germany (1989).
37. T. A. Ramanarayanan and R. A. Rapp, *Metall. Trans.*, **3**, 3239 (1972).
38. W. Eichenauer and G. Muller, *Z. Metallkd.*, **53**, 321 (1962).
39. *1997 Annual Book of ASTM Standards*, Vol. 03.01, p. 227, The American Society for Testing and Materials, West Conshohocken, PA (1997).
40. JCPDS Card File, Cards 28-156, 4-783, 7-233, 22-1056, 45-1471, 22-1054, 44-585, and 27-1402.
41. C. L. White and C. T. Liu, *Acta Metall.*, **29**, 301 (1981).
42. H. Kleykamp, *J. Less-Common Met.*, **63**, 25 (1979).